# Effects of copper nanoparticles on rat cerebral microvessel endothelial cells

**Article** *in* Nanomedicine · February 2012

DOI: 10.2217/nnm.11.154 · Source: PubMed



**11 authors**, including:

Susan Lantz
U.S. Food and Drug Administration
**26** PUBLICATIONS **521** CITATIONS
SEE PROFILE

Amanda M Schrand
University of Dayton
**46** PUBLICATIONS **5,335** CITATIONS
SEE PROFILE

Bonnie L Robinson
U.S. Food and Drug Administration
**25** PUBLICATIONS **766** CITATIONS
SEE PROFILE

John J Schlager
Air Force Research Laboratory
**95** PUBLICATIONS **10,063** CITATIONS
SEE PROFILE

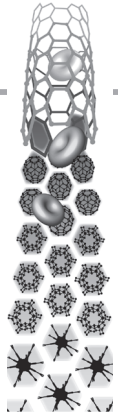



# Effects of copper nanoparticles on rat cerebral microvessel endothelial cells

**Aim:** The purpose of the current study was to determine whether copper nanoparticles (Cu-NPs) can induce the release of proinflammatory mediators that influence the restrictive characteristics of the blood–brain barrier. **Material & methods:** Confluent rat brain microvessel endothelial cells (rBMECs) were treated with well-characterized Cu-NPs (40 or 60 nm). Cytotoxicity of the Cu-NPs was evaluated by cell proliferation assay (1.5–50 µg/ml). The extracellular concentrations of proinflammatory mediators (IL-1β, IL-2, TNF-α and prostaglandin $E_2$) were evaluated by ELISA. **Results:** The exposure of Cu-NPs at low concentrations increases cellular proliferation of rBMECs, by contrast, high concentrations induce toxicity. Prostaglandin $E_2$ release was significantly increased (threefold; 8 h) for Cu-NPs (40 and 60 nm). The extracellular levels of both TNF-α and IL-1β were significantly elevated following exposure to Cu-NPs. The P-apparent ratio, as an indicator of increased permeability of rBMEC was approximately twofold for Cu-NPs (40 and 60 nm). **Conclusion:** These data suggest that Cu-NPs can induce rBMEC, proliferation at low concentrations and/or induce blood–brain barrier toxicity and potential neurotoxicity at high concentrations.

Original submitted 9 June 2011; Revised submitted 1 August 2011; Published online 16 February 2012

**KEYWORDS: blood–brain barrier ■ copper nanoparticle ■ neuroinflammation ■ neurotoxicity ■ rat brain microvessel endothelial cell**

**William J Trickler[1], Susan M Lantz[1], Amanda M Schrand[2], Bonnie L Robinson[1], Glenn D Newport[1], John J Schlager[2], Merle G Paule[1], William Slikker[1], Alexandru S Biris[3], Saber M Hussain[2] & Syed F Ali*[1]**

*[1]Neurochemistry Laboratory, Division of Neurotoxicology, HFT-132, National Center for Toxicological Research/FDA 3900 NCTR Road, Jefferson, AR 72079, USA*

*[2]Applied Biotechnology Branch (711 HPW/RHPB), Human Effectiveness Directorate, Air Force Research Laboratory, Wright-Patterson AFB, OH 45433-5707, USA*

*[3]University of Arkansas at Little Rock, Little Rock, AR 72079-9502, USA*

**Author for correspondence:*
*Tel.: +1 870 543 7123*
*Fax: +1 870 543 7745*
*syed.ali@fda.hhs.gov*

At present, various metal oxide nanoparticles are used in the manufacturing of hundreds of commercial products. Copper oxide (CuO) nanoparticles (Cu-NPs) are used in antimicrobial preparations, heat transfer fluids, semiconductors, intrauterine contraceptive devices, polymers/plastics, metallic coatings, inks and lubricant additives [1]. As a lubricant additive, Cu-NPs effectively reduce friction and wear, or repair worn surfaces. Given the significant increase in manufacturing and industrial uses of nanomaterials, Cu-NPs are likely to not only enter the environment, but also result in human exposures. The impact of such exposures on human health must be carefully evaluated. A vital part of addressing the safety of these nanomaterials is gaining a clear understanding of how biological systems respond to the exposure of nanomaterials. The exact physicochemical nature of NPs in biological systems is not fully described or understood at this time, and there are some significant challenges in assessing NP behavior at the biointerface, as recently reviewed by our group [2]. However, the proper characterization of NPs is essential to assess physicochemical characteristics such as: size, surface chemistry, crystallinity, morphology, solubility, aggregation tendency, uptake and localization, which are linked to various degrees of the resultant NP toxicity.

In this study, we examined Cu-NPs that have demonstrated high toxicities in various cell and animal models, which have recently been reviewed elsewhere [3]. With respect to the blood–brain barrier (BBB) function and neurotoxicity, studies have shown that Cu-NPs introduced into the systemic blood supply can induce BBB dysfunction, astrocyte swelling and neuronal degeneration [4,5]. However, a comprehensive understanding at the cellular level of how Cu-NPs induce BBB dysfunction and neurotoxicity remains largely unknown.

The BBB is a highly specialized vascular barrier that tightly regulates the passage of substances from the systemic blood supply into the CNS. Previous studies have shown immunological, chemical or physical insult can cause increased BBB permeability resulting in BBB dysfunction, which is correlated with the release of proinflammatory cytokines, TNF-α, IL-1β and several second messengers, including vasodilators such as prostaglandin $E_2$ ($PGE_2$) and nitric oxide both *in vitro* [6–11] and *in vivo* [6–8,12–15]. Activation of cerebral microvasculature, release of proinflammatory signals (i.e., cytokines) and BBB dysfunction can markedly affect brain functions [16]. Therefore,

Future Medicine part of fsg

evaluating how the cerebral microvasculature responds to nanomaterials is critical in understanding the potential neurotoxicity related to exposure.

Primary brain microvessel endothelial cells (BMECs) isolated from cerebral cortices grow polarized cell monolayers representative of the BBB and provide a well-suited *in vitro* model for evaluating BBB permeability, transport characteristics and associated molecular mechanisms [17–20]. To evaluate whether Cu-NP exposure produces proinflammatory-mediated cerebral microvascular activation and potential toxicity, this *in vitro* model was used in the current study. Previous studies demonstrated that smaller silver NPs (25 and 40 vs 80 nm) produced stronger activation of rat BMECs (rBMECs) involving the significant release of proinflammatory mediators ($PGE_2$, TNF-α and IL-1β) associated with morphological changes correlated with increased BBB permeability [21]. In other studies using this model, gold NPs (3, 5, 7, 10, 30 and 60 nm) were shown to cause only mild permeability changes and activation of rBMECs [22]. Therefore, a clear understanding of how the cerebral microvasculature responds to nanomaterials is of considerable importance for assessing the potential neurotoxicity risks associated with them. The current study evaluated the cellular proinflammatory mediator responses, changes in cellular morphology and permeability following exposure to various sized Cu-NPs. To our knowledge, the involvements of proinflammatory-mediated changes in rBMEC integrity and changes in BBB permeability *in vitro* in response to Cu-NPs have not been reported previously.

## Materials & methods

### Materials & statistics

Cu-NPs (40 and 60 nm) were a kind gift from Karl Martin of NovaCentrix, TX, USA (formerly Nanotechnologies, Inc.). ELISA kits for $PGE_2$, TNF-α, IL-1β and IL-2 were purchased from R&D Systems (MA, USA). All remaining media, media supplements and reagents were obtained from Sigma-Aldrich (MO, USA). Statistical analyses of the various treatment effects were determined using nonparametric Kruskal–Wallis analysis of variance with Tukey multiple *post hoc* comparisons of means. For all studies, statistical significance was designated as $p < 0.05$.

### Cu-NP characterization

Powder x-ray diffraction was used to characterize the chemical composition of the Cu-NPs. Briefly, Cu-NPs were sprinkled onto slides coated with silicone grease prior to analysis on a Rigaku 2500 x-ray diffraction unit. All of the data was acquired under the following parameters: divergence slit = scatter slit = 1°; divergence height limiting slit = 10 mm; and receiving slit = 0.6 mm. Powders were scanned in 2θ–θ geometry (also known as Bragg–Brentano geometry) from 2θ 20° to 100°. The sampling interval was 0.05° and the scan speed was 3° per min. We used a continuous scan. The power parameters were 50 kV, 300 mA and 15 kW.

Bright-field transmission electron microscopy (TEM) was used to observe the morphology of the NPs. Briefly, suspensions of Cu-NPs were prepared in water, then drop-cast onto formvar-coated TEM grids. Images to demonstrate NP size and morphology were performed on a Hitachi H-7600 tungsten-tip high-resolution TEM instrument at an accelerating voltage of 100 kV and associated Active Management Technology software was used to collect digital images. Enlargements of selected areas were performed by cropping and enlargement of high-resolution images in Microsoft® Powerpoint.

The surface charge of the Cu-NPs in solution was determined using laser doppler velocimetry (Malvern Instruments Zetasizer Nano-ZS, MA, USA). Samples were examined after dilution of NP stock solutions to 100 µg/ml suspensions in deionized water, vortexed to provide a homogeneous solution and then 1 ml was transferred to a Malvern Clear Zeta Potential Cell for laser doppler velocimetry measurements (water dispersion) as previously described [2].

### Cell isolation & culturing of primary rBMECs

The rBMECs were isolated by a modified method previously described [17]. Briefly, the gray matter of fresh rat cerebral cortices was mechanically homogenized through a 100-µm mesh screen after the meninges were removed. Dispase II enzyme (5 mg/ml) reconstituted in miniumum essential medium (MEM) isolation media (1 M, 4-[2-hydroxyethyl]-1-piperazineethanesulfonic acid [HEPES; 50 mM], polymyxin B [50 µg/ml], gentamicin [50 µg/ml], amphotercin B [2.5 µg/ml] at pH 7.4) was added to the freshly homogenized cerebral cortical tissue (10 mg/g brain tissue) and MEM isolation media at pH 9.0 was added (equal w/w of brain tissue). The mixture was placed in an incubated shaker for 1 h (37°C at 150 × g).

Following this incubation, the supernatant was removed by centrifugation (10 min at 1570 × g). The crude capillaries were isolated by resuspending the cerebral cortical tissue in a solution (13% [w/v] dextran supplemented with MEM [1 M], HEPES [50 mM], gentamicin [40 µg/ml], polymyxin B [50 µg/ml] and amphotericin B [2.5 µg/ml]) followed by centrifugation (10 min at 9170 × g). The crude capillary pellet was collected and resuspended in a collagenase/dispase (5 mg/ml) solution at a final concentration of 0.1% (v/w) and placed in an incubated shaker (37°C at 150 rpm) for 1 h. During this time a percoll gradient (50% final concentration, supplemented with MEM [1 M], HEPES [50 mM], gentamicin [40 µg/ml], polymixin B [50 µg/ml] and amphotercin B [2.5 µg/ml]) was set up by centrifugation (60 min at 39,200 × g). The digested capillaries were centrifuged (10 min at 1700 × g) to remove the enzymatic treatment and resuspended in isolation media and pipetted into the percoll gradient tubes. The rBMECs were then separated by centrifugation (10 min at 1700 × g). The freshly isolated rBMECs were extracted from the percoll gradient (3 cc syringe), pelleted and resuspended in rBMECs complete media (45% [v/v] MEM; 45% [v/v] Ham's F-12 nutrient mix, supplemented with 10 mM HEPES, 13 mM sodium bicarbonate, 50 µg/ml gentamicin, 20% [v/v] fetal bovine serum, 2.5 µg/ml amphotericin B, and 100 µg/ml sodium heparin). The rBMECs were plated (~50,000 cells/cm$^2$ density) on collagen-coated, fibronectin-treated culture plates and incubated in a humidified incubator (37°C with 5% [v/v] $CO_2$). The cells were used after reaching confluence, typically 8–12 days.

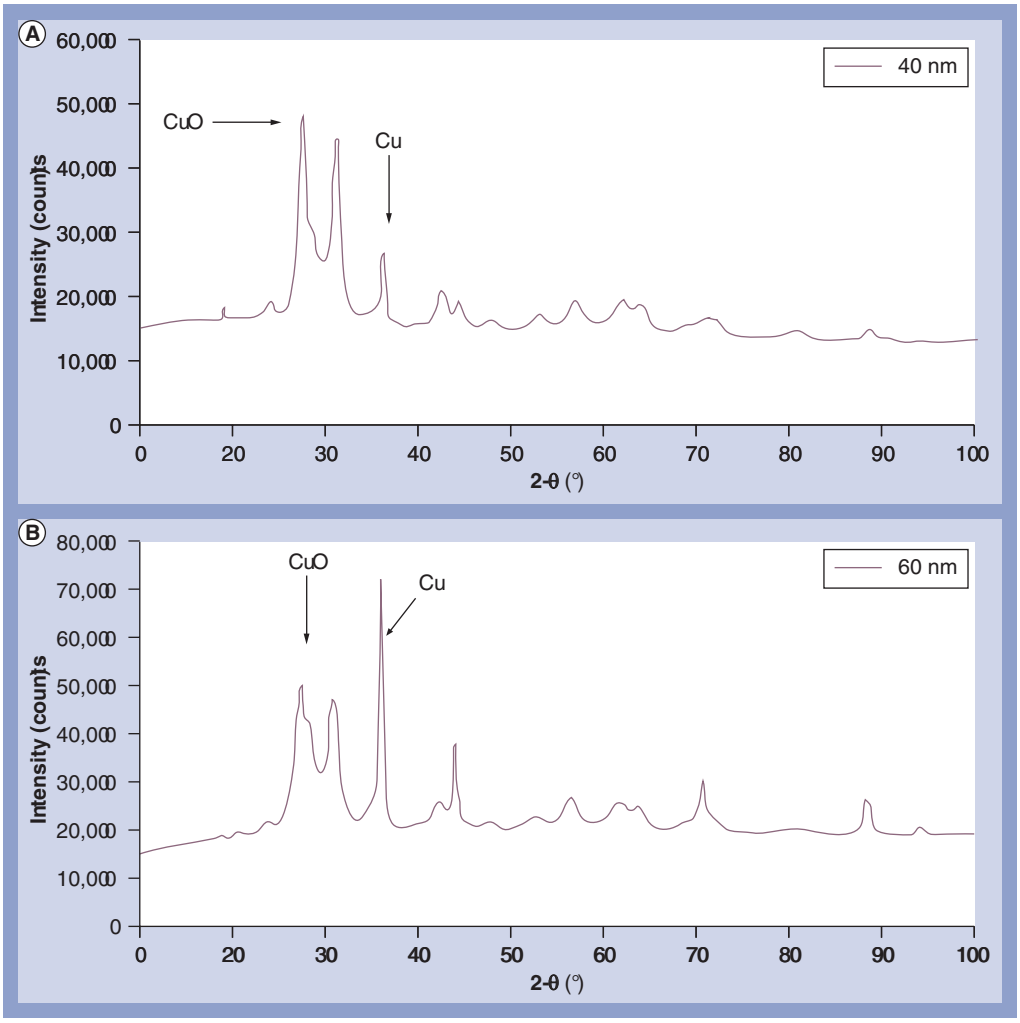


**Figure 1. Powder x-ray diffraction of copper nanoparticles. (A)** 40-nm and **(B)** 60-nm Cu nanoparticles. Both samples of Cu nanoparticles contained substantial amounts of CuO. The greatest amount of oxidized Cu was observed in **(A)** the 40-nm sample compared with **(B)** the 60-nm sample. Cu: Copper; CuO: Copper oxide.

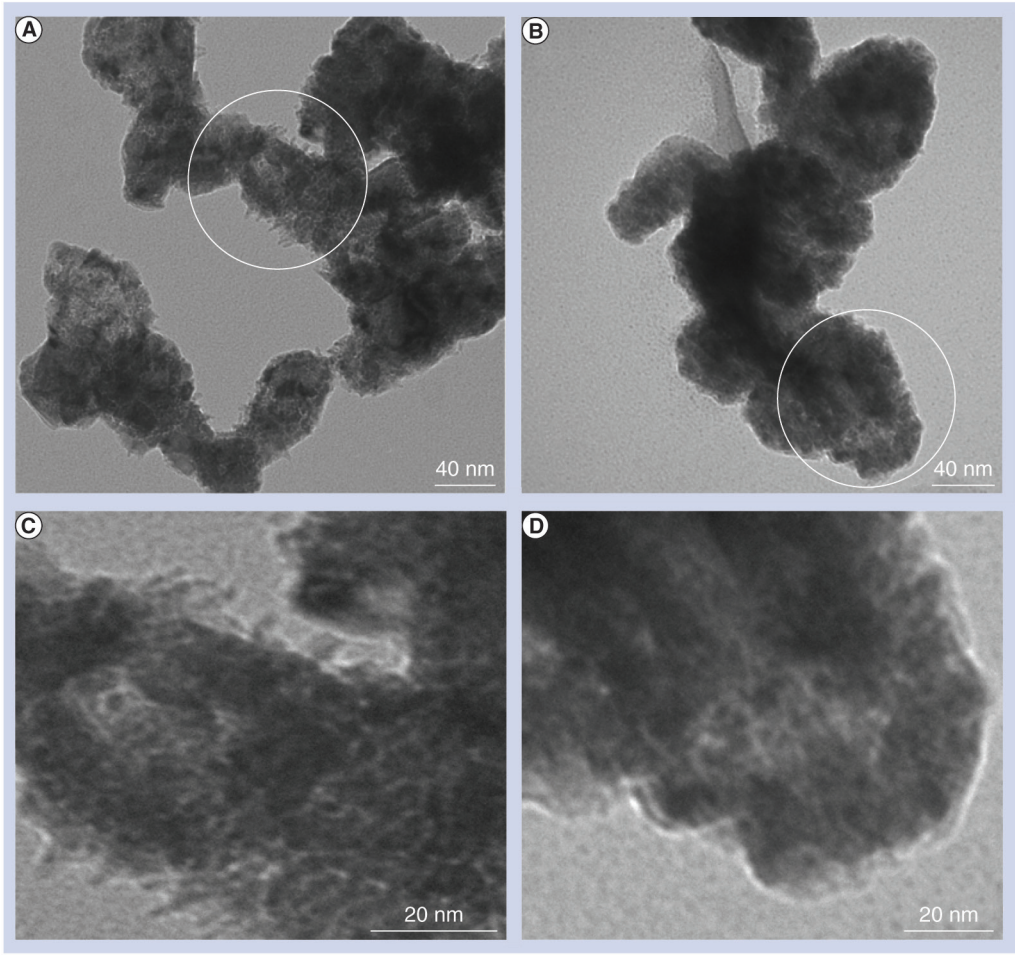


**Figure 2. Bright-field transmission electron microscope images of copper nanoparticles showing approximate size and morphology. (A)** 40-nm copper nanoparticles (Cu-NPs) and **(B)** 60-nm Cu-NPs. **(C & D)** These are enlargements of the circled areas in **(A & B)**, respectively, to show surface detail, noting the appearance of surface oxidation on the Cu-NPs.

## Viability assay for Cu-NPs in primary rBMECs

The viability of rBMECs were determined using 2,3-bis(2-methoxy-4-nitro-5-sulfophenyl)-2H-tetrazolium-5-carboxanilide cytotoxicity analyses. Briefly, the cells were seeded in a 96-well cell culture plate at a density of 5000 cells per well in 100 µl of complete growth media and cultured (8–12 days) in complete growth media. The cells were treated with various concentrations (0.8–50 µg/ml) in a single bolus with a solution of Cu-NPs (40 or 60 nm) for 24 h, then gently washed three-times with ice cold phosphate buffer solution (pH 7.4) and supplied with fresh growth media (130 µl/well) containing fresh 2,3-bis(2-methoxy-4-nitro-5-sulfophenyl)-2H-tetrazolium-5-carboxanilide reagent (300 µg/ml) and phenazine methosulfate (37.5 µM final concentration) and further incubated for 2 h at ambient temperature. The absorbance was determined using a microplate reader at 450 nm with reference wavelength of 650 nm. The absorbance data was analyzed and presented as survival percentage of control monolayers receiving media alone.

## $PGE_2$ release from primary rBMECs

The release of $PGE_2$ from the rBMEC monolayers was determined using a $PGE_2$-specific ELISA kit (R&D Systems). Cross-reactivity for other prostaglandins was 70, 16.3, 1.4 and 0.7% for $PGE_1$, $PGE_3$, $PGF_{1\alpha}$ and $PGF_{2\alpha}$, respectively. Confluent rBMEC monolayers grown on six-well culture plates were placed in fresh complete culture media (2 ml) 24 h prior to Cu-NP exposure. Media was sampled (50 µl) at various time points following Cu-NP exposure (0–8 h) for use in the $PGE_2$ ELISA. The amount of $PGE_2$ released into the culture media was standardized based on the protein content of the cell monolayers, as determined by the Bradford colorimetric assay. The results are presented as the average amount of $PGE_2$ per mg of protein.

### Cytokine release from primary rBMECs

The release of TNF-α, IL-1β and IL-2 in response to Cu-NP exposure was determined in rBMEC monolayers. The cytokines were measured using commercially available ELISA kits (R&D Systems). Cross-reactivity for TNF-α and IL-1β from other species and other cytokines was not observed, and the limit of detection was less than 6 and 15 pg/ml, respectively. Confluent rBMEC monolayers grown on six-well culture plates were placed in fresh complete culture media (2 ml) 24 h prior to the experiment. Media was sampled (50 µl) at various time points following NP exposure (0–8 h) and processed as described in the ELISA protocol. Concentrations of TNF-α, IL-1β and IL-2 released into the culture media were corrected for the amount of cellular protein as determined by the Bradford colorimetric protein assay. The results were presented as the average amount of cytokine per mg of protein.

### Cu-NP exposure effects permeability in primary rBMECs

The effects of Cu-NPs on the permeability of primary rBMEC monolayers were determined using methods that have been previously described [9,21–23]. Briefly, the freshly isolated rBMECs were plated in triplicates (50,000 cells/cm$^2$ seeding density) on collagen-coated, fibronectin-treated polycarbonate membrane inserts and cultured until confluence (12 mm; 0.4-µm pore size, Costar Transwell™ 12-well, MA, USA). Complete culture media for confluent rBMEC monolayers was replaced 24 h prior to the start of the experiment. The Cu-NPs were diluted in complete culture media and spiked into the apical chamber (15 µg/ml final concentration) and incubated for 24 h in a humidified incubator supplemented with 5% $CO_2$ at 37°C. Following the 24-h exposure period, the treatment media was removed from both apical and basolateral sides and replaced with fresh assay II buffer with (apical) or without (basolateral) fluorescein (10 µM). Samples (100 µl) were removed from the basolateral compartment at various times (0–90 min) and replaced with fresh buffer. The concentration of fluorescein in the samples was determined using a Chameleon microplate spectrophotofluorometer (485-nm excitation and 530-nm emission wavelengths). Permeability was expressed as the flux percentage of the fluorescein marker across the rBMEC monolayers over time (mean ± standard deviation, n = 3). The apparent permeability coefficients were calculated as previously described using Equation 1 [24]:

$$P_{app} = \frac{1}{AC_0} \cdot \frac{dQ}{dt} \quad (1)$$

Where, dQ/dt is the flux across the cell monolayers, A is the surface area of the membrane and $C_0$ is the initial concentration of fluorescein.

## Results

### Cu-NP characterization

Powder x-ray diffraction analysis demonstrated that both 40- and 60-nm sized Cu-NPs contained substantial quantities of CuO (Figure 1). The 40-nm powder may actually be primarily composed of CuO rather than elemental Cu, based on the fact that the largest CuO peak was more than twice as high as the main Cu peak. The 60-nm Cu-NPs had a higher ratio of Cu to CuO. One explanation for the inverse relationship between Cu-NP size and oxide content (i.e., the copper oxide content is greater in the 40-nm Cu-NPs compared to the 60-nm Cu-NPs) is that the 40-nm Cu-NPs have the highest surface area to volume ratio and, therefore, the greatest propensity for potential surface oxidation. The four possible phases in the Cu-NP samples were identified as Cu (Copper JCPDS file 04-0836), CuO (unknown structure JCDPS file 44-706), CuO (Tenorite JCDPS file 48-1548tenorite) and $Cu_2O$ (Cuprite synthetic JCPDS file 05-0667). The $Cu_2O$ (cuprite) peaks were very small, therefore, if it was actually present, it was a small amount. The CuO phases listed have fairly similar peaks and may actually be tenorite but with some impurities.

The size and morphology of 40- and 60-nm sized Cu-NPs were examined with bright-field TEM (Figure 2). Very strong aggregates were noticeable precluding a definitive size measurement, although diameters were estimated to increase with increasing size. The presence of surface oxidation on all of the Cu-NP samples was evident. Further characterization of the surface charge of the Cu-NPs revealed negative zeta potentials ranging from -30 to -50 mV (Table 1).

**Table 1. Surface charge of copper nanoparticles.**

| Copper nanoparticle sample | ζ-potential |
|---|---|
| 40-nm copper nanoparticles | -47.6 mV |
| 60-nm copper nanoparticles | -36.6 mV |

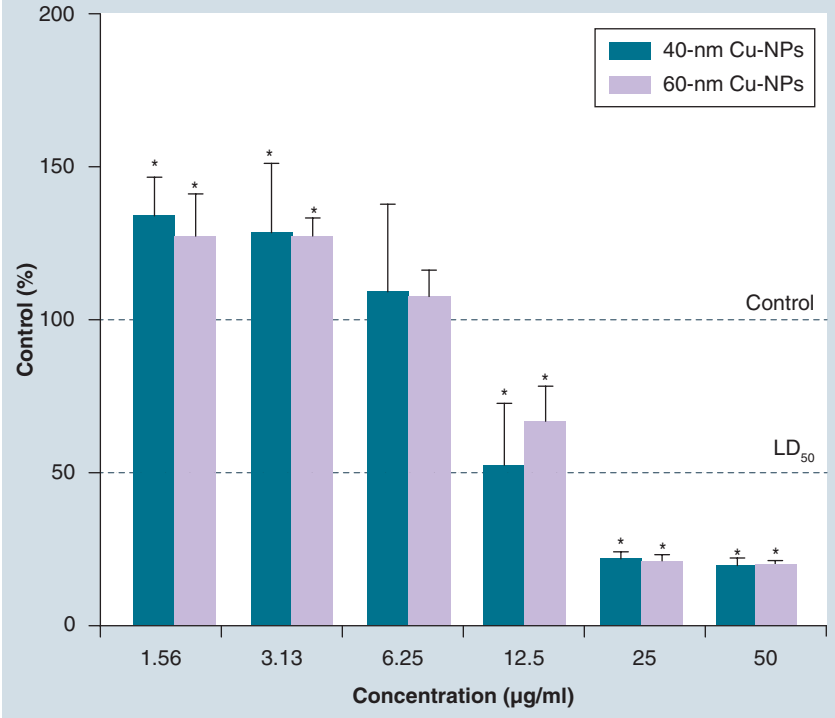


**Figure 3. The effects of copper nanoparticles on the cellular proliferation of primary rat brain microvessel endothelial cells.** Triplicate cell monolayers were treated with a concentration range (0.8–50 µg/ml) of Cu-NPs: 40 nm, 60 nm or control (media alone). The data are presented as percentage of control (treatment/control; mean ± standard deviation; n = 3).
*Considered statistically significant ($p < 0.05$) from control.
Cu-NP: Copper nanoparticle; $LD_{50}$: Lethal dose for 50%.

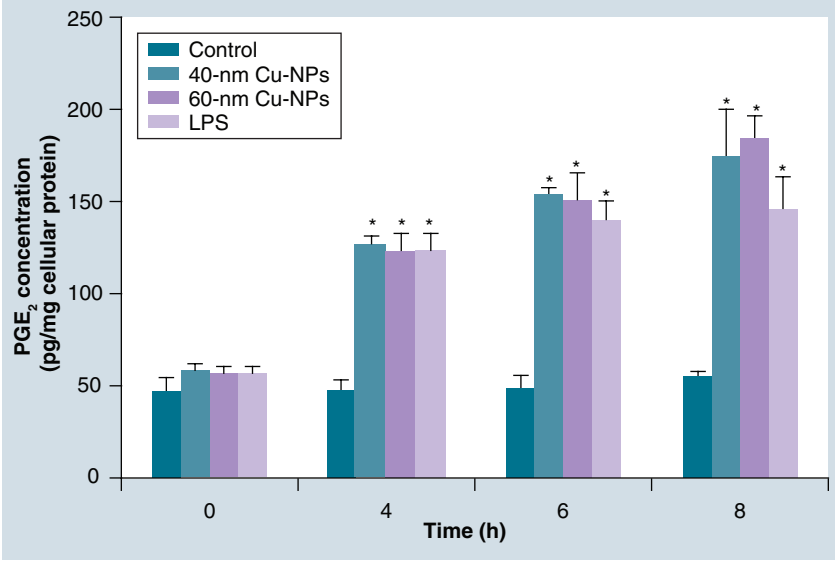


**Figure 4. The effects of copper nanoparticles on the release of prostaglandin $E_2$.** Triplicate cell monolayers were treated with Cu-NPs (25 µg/ml); control (media alone), 40-nm Cu-NPs, 60-nm Cu-NPs and positive control LPS (10 µg/ml). The data are presented as mean ± standard deviation; n = 3.
*Considered statistically significant ($p < 0.05$) from control.
Cu-NP: Copper nanoparticle; LPS: Lipopolysaccharide; $PGE_2$: Prostaglandin $E_2$.

## The effects of Cu-NPs on cellular proliferation in primary rBMECs

The effects of Cu-NPs on rBMEC cellular proliferation are presented as percentage of control (mean ± standard deviation) of triplicate primary rBMECs for specific-sized Cu-NPs (40 or 60 nm) following 24-h exposure (Figure 3). With respect to cell proliferation, Cu-NPs have a biphasic concentration profile over the range tested: low concentrations (~3.13 µg/ml and below) significantly increased the cellular proliferation for both sized particles. Conversely, higher concentrations (~12.5 µg/ml and above) significantly reduced cellular proliferation for both sized Cu-NPs (Figure 3). The observed lethal dose for 50% was approximately 12.5 µg/ml for both sized Cu-NPs.

## The effects of Cu-NPs on the release of $PGE_2$

The release of $PGE_2$ from the rBMEC monolayers was evaluated at various time intervals (0–8 h) following exposure to Cu-NPs (40 and 60 nm) or lipopolysaccharide (LPS) as a positive control. The data (mean ± standard deviation) are presented as $PGE_2$ concentration per mg of total cellular protein (Figure 4). The exposure to either 40- or 60-nm Cu-NPs or LPS (10 µg/ml) produced significant increases in extracellular levels of $PGE_2$ (threefold) when compared with the control as early as 4 h. These significantly elevated levels of $PGE_2$ persisted for all exposure groups when compared with the control over the duration of the experiment period (8 h).

## The effects of Cu-NPs on the extracellular concentrations of cytokines

The time-release profiles for TNF-α, IL-1β and IL-2 were determined in rBMEC monolayers in response to specific-sized Cu-NPs (40 and 60 nm) or LPS (10 µg/ml) as a positive control, and the data are presented as mean ± standard deviation cytokine concentration per mg of the total cellular protein (Figures 5 & 6; data for IL-2 not shown). Significant amounts (~twofold) of TNF-α were released from the rBMECs following treatment with both 40- and 60-nm Cu-NPs and LPS at 4 h postexposure (Figure 5). The secretion of TNF-α further increased (~threefold) with both 40- and 60-nm Cu-NPs and LPS over the duration of the experimental period (8 h). The extracellular levels were significantly increased (at least twofold) at 4 h postexposure for both 40- and 60-nm Cu-NPs and LPS when compared with control monolayers (Figure 6). However, by

6 h postexposure, the treatment with both sized Cu-NPs further increased the extracellular levels of IL-1β (at least fourfold) (Figure 6). By 8 h post-treatment, the release of IL-1β from rBMECs was robust in response to both sized Cu-NPs and LPS with a magnitude of approximately fivefold (Figure 6). The release of IL-2 from the rBMEC monolayers in response to Cu-NPs or LPS was unremarkable over the experimental period examined (data not shown).

### Morphology of rBMECs following exposure to Cu-NPs

Representative cell monolayers were treated with Cu-NPs or copper nitrate (15 µg/ml) for 24 h (Figure 7). The micrographs of rBMECs following treatment with Cu-NPs exhibited significant morphological changes (Figures 7C & 7D) when compared with control monolayers after 24 h of exposure (Figure 7A). The cell monolayers appear significantly stressed with the appearance of abnormal extracellular gaps and rounded cells. Morphological changes in the rBMECs following the exposure of copper nitrate (control for elemental Cu) (Figure 7B) were indistinguishable from the control (Figure 7A).

### Cu-NP exposure affects permeability of rBMECs

The permeability was determined by evaluating the transport of fluorescein across rBMECs following apical (blood-side) exposure to Cu-NPs (40 and 60 nm; 15 µg/ml) for 24 h (Figure 8). Both sized Cu-NPs significantly increased the permeability of fluorescein across the rBMEC monolayers over the 90-min experimental time frame. The magnitude of the effect was approximately twofold. The significant increase in permeability to fluorescein was further evidenced by the significant changes in the apparent permeability coefficients for both 40- and 60-nm Cu-NPs (Table 1).

## Discussion

With the increased production and industrial use of nanomaterials, it is becoming increasingly important to public health that we understand how biological systems respond to them. Chen *et al.* evaluated the toxicity of Cu-NPs (23.5 nm) and Cu-microparticles following oral administration *in vivo*, and found the kidney, liver and spleen to be target organs for significant toxicological effects and heavy injuries for Cu-NPs but not Cu-microparticles [25]. In addition, Liu *et al.* demonstrated significant pathological changes in body weight, hydropic degeneration around the central vein and necrosis of the liver hepatocyes, as well as significant lesions in the olfactory bulbs and kidneys of animals treated with intranasal Cu-NPs (three doses of 40 mg/kg in 1 week) [26]. These studies further evaluated the retention and distribution of Cu in various tissues by inductively coupled plasma

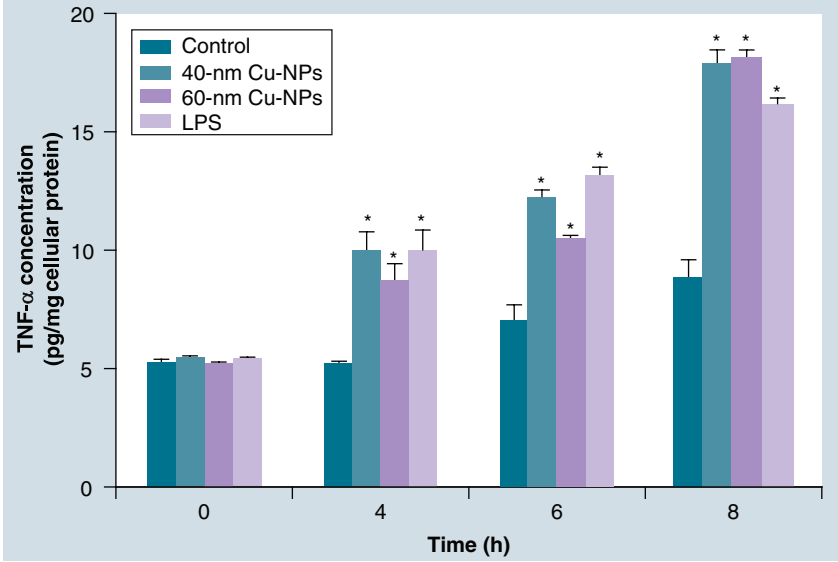


**Figure 5. The effects of copper nanoparticles on the release of TNF-α.**
Triplicate cell monolayers were treated with Cu-NPs (25 µg/ml); control (media alone), 40-nm Cu-NPs, 60-nm Cu-NPs and positive control LPS (10 µg/ml). The data are presented as mean ± standard deviaition; n = 3.
*Considered statistically significant ($p < 0.05$) from control.
Cu-NP: Copper nanoparticle; LPS: Lipopolysaccharide.

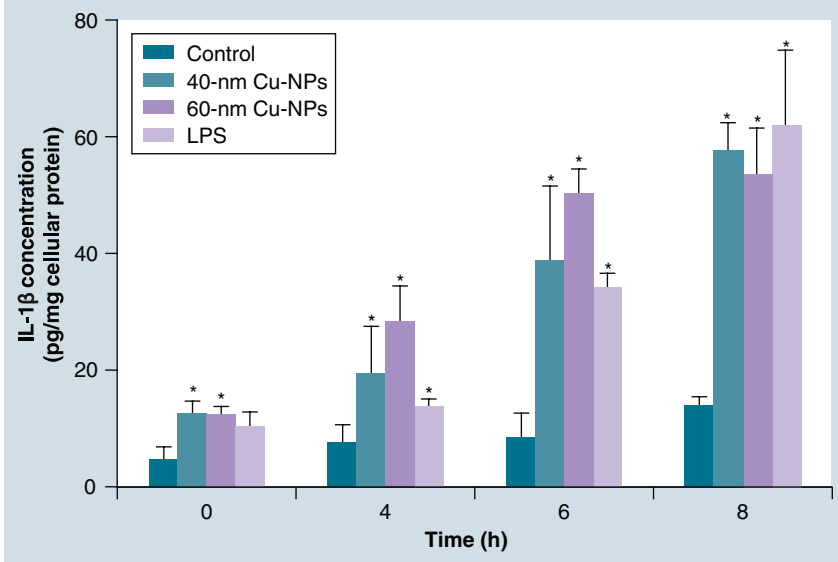


**Figure 6. The effects of copper nanoparticles on the release of IL-1β.**
Triplicate cell monolayers were treated with Cu-NPs (25 ug/ml); control (media alone), 40-nm Cu-NPs, 60-nm Cu-NPs and positive control LPS (10 µg/ml). The data are presented as mean ± standard deviation: n = 3.
*Considered statistically significant ($p < 0.05$) from control.
Cu-NP: Copper nanoparticle; LPS: Lipopolysaccharide.

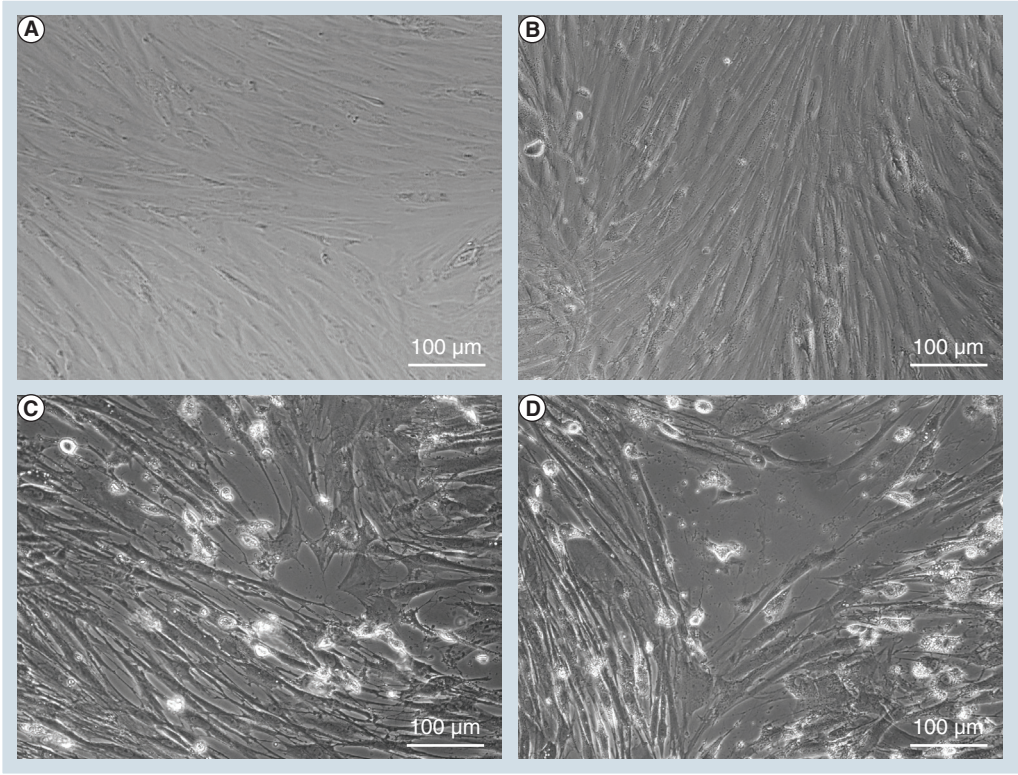


**Figure 7. Morphology of rat brain microvessel endothelial cells following exposure to copper nanoparticles.** Representative cell monolayers were treated with copper nanoparticles (Cu-NPs; 15 µg/ml) for 24 h. **(A)** Control (media alone); **(B)** copper nitrate; **(C)** 40-nm Cu-NPs; and **(D)** 60-nm Cu-NPs. Micrographs are at 20× magnification.

mass spectrometry demonstrating that the liver, kidneys and olfactory bulb are the main accumulated tissues for Cu-NPs [26]. Within the cells of the CNS, Prabhu *et al.* showed that Cu-NPs disrupted neurite networks in rat somatosensory neurons in the CNS as evidenced by the presence of vacuoles and the detachment of some neurons from the substratum. They further suggested that the significant toxic effects observed with a variety of sizes of Cu-NPs were attributable to the production of reactive oxygen species (ROS) [27]. Other studies have indicated that Cu can be metabolized in hepatoma tissue culture cells, and be transferred to metallothionein (where Cu is stored) by reduced glutathione (GSH). When Cu overload is reached, it is thought by some that depletion of GSH can instantaneously result in enhanced cellular toxicity [28–31]. These reports along with those from other researchers have consistently demonstrated that Cu ions can lead to increased ROS production and ROS-induced inflammation in biological tissues.

Fahmy and Cormier demonstrated that Cu-NPs were able to overwhelm antioxidant defenses (e.g., catalase and GSH reductase), increasing the levels of 8-isoprostanes and the ratio of GSH disulfide to total GHS in HEp-2 cells, and that cotreatment with the antioxidant resveratrol increased cell viability suggesting that oxidative stress was the cause of exposure-associated cytotoxic effects [32]. Karlsson *et al.* demonstrated by commet assay in a human lung epithelial cell line, A549, that Cu-NPs were most potent compared with the Cu ions regarding cytotoxicity and DNA damage attributed to significant increases in intracellular ROS as measured by the oxidation-sensitive fluoroprobe 2',7'-dichlorofluorescin diacetate [33]. This suggested that the observed toxicity was probably not explained by Cu ions released into the cell medium. Karlsson *et al.* further showed a clear dose response in mitochondrial depolarization as the potential mechanism behind the toxicity of Cu-NPs in A549 cells [34]. It is well known that damage to the mitochondria can trigger apoptosis. Mitochondrial depolarization may be due to structural damage following particle interactions, which has been shown by ultrafine particles that lodge in the mitochondria [35]. The structural damage leads to loss of mitochondrial membrane potential, opening of the permeability transition pore, ROS

production and cell death [36]. Together these previous studies establish a positive correlation between Cu-NPs and Cu ions leading to ROS-induced inflammation in peripheral organ tissues and neuronal cells tissues. However, the biological interactions of Cu-NPs with the vascular endothelial tissue remain largely unknown. In addition, the release of proinflammatory cytokines following cerebral microvasculature damage has been linked to oxidative free-radical generation and growth factors [37–41].

Therefore, the present study focuses on the cerebral microvasculature to clarify the increased permeability following exposure to Cu-NPs and the involvement of proinflammatory mediators. With respect to BBB function and neurotoxicity, the reports are limited. These limited studies have shown that Cu-NPs introduced into the systemic blood supply can induce BBB dysfunction, astrocyte swelling and neuronal degeneration *in vivo* [4]. Sharma *et al.* demonstrated the leakage of Evan's blue dye and radioiodine in the rat brain following intravenous (30 mg/kg) or intraperitoneal (50 mg/kg) administration of Cu-NPs [4]. Sharma *et al.* further suggested that the increased cerebral microvasculature permeability involves ROS generation because the increased permeability was attenuated by nanowire–antioxidant therapy following chronic exposure of Cu-NPs *in vivo* [5]. Although increased BBB permeability has been shown, little is known about the responses at the cellular level following Cu-NPs exposure. Therefore, the current report identifies a time-dependent proinflammatory response induced by Cu-NPs at the cellular level in rBMECs, which is further evidenced by the increased BBB permeability of fluorescein. To our knowledge, this report is the first to evaluate the proinflammatory response and integrity of the BBB *in vitro* following exposure to Cu-NPs.

With respect to the responses in the cerebral microvasculature that have been shown to induce alterations in BBB integrity discussed previously, there are several lines of evidence supporting these results in this report. In the current study, the exposure of Cu-NPs induced the increased production of various proinflammatory mediators (TNF-α, IL-1β and $PGE_2$). The time-dependent profile and increased release of these particular proinflammatory mediators significantly correlate with the increased rBMEC permeability following exposure to Cu-NPs, and further suggest that morphological changes in rBMEC monolayer integrity are associated with increased permeability. With respect to cellular morphological changes, the current study also clearly demonstrates alterations in cellular morphology following exposure to Cu-NPs in rBMECs. The interactions of the Cu-NPs with rBMECs induce cellular damage in the observed monolayers with the appearance of perforations in the monolayers at concentrations around the lethal dose 50% and above. The observed perforations appear to be independent of the size of Cu-NPs at the concentration

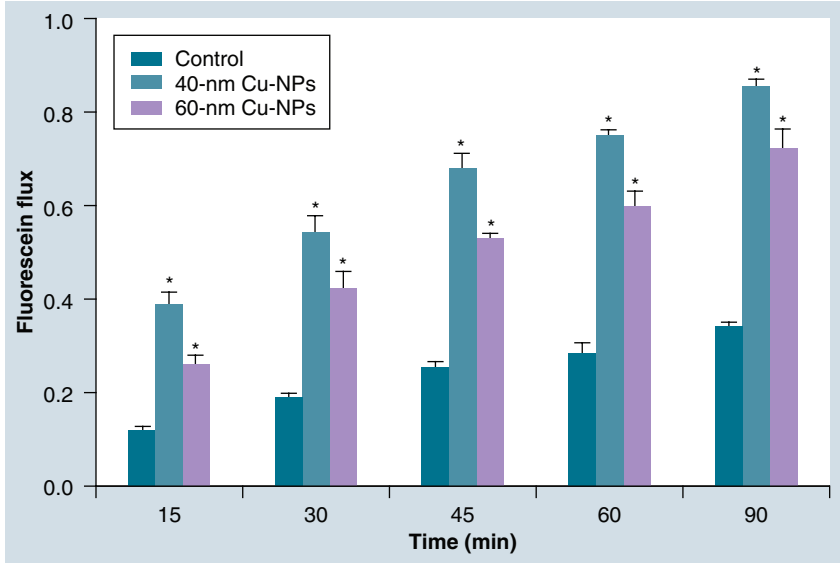


**Figure 8. Copper nanoparticle exposure affects permeability in rat brain microvessel endothelial cells.** Triplicate cell monolayers were treated with Cu-NPs (15 μg/ml); control (media alone), 40-nm Cu-NPs, 60-nm Cu-NPs. The data are expressed as fluorescein transport (mean ± standard deviation: n = 3).
*Considered statistically significant ($p < 0.05$) from control.
Cu-NP: Copper nanoparticle.

**Table 2. Apparent permeability changes following copper nanoparticle exposure.**

| Treatment groups | Apparent permeability coefficient ($1 \times 10^{-6}$ cm/s) | Apparent permeability coefficient ratio (treatment/control) |
|---|---|---|
| Control | 1.55 ± 0.110 | 1.02 ± 0.082 |
| 40-nm Cu-NPs | 3.27 ± 0.297* | 2.17 ± 0.221* |
| 60-nm Cu-NPs | 3.17 ± 0.209* | 2.08 ± 0.155* |

*Calculated by: where, dQ/dt is the flux across the cell monolayers, A is the surface area of the membrane and $C_0$ is the initial concentration of fluorescein. The data are presented as mean ± standard deviation.*
**Considered statistically different from control monolayers ($p < 0.05$; n = 3).*
*Cu-NP: Copper nanoparticle.*

tested (Figures 7C & 7D) when compared with control (Figure 7A). The morphology changes in the rBMECs following the exposure of Cu-NPs were further evidenced by significantly increasing the fluorescein permeability compared with monolayers treated with Cu-NPs (Figure 8 & Table 2). Furthermore, the permeability changes associated with the exposure to Cu-NPs also correlate well with the release patterns of proinflammatory mediators in this report (Figures 4–6). Together, the time profile for the release of $PGE_2$, TNF-α and IL-1β clearly show both Cu-NPs (40 and 60 nm) produced profound effects on the release of proinflammatory mediators from rBMECs at high concentrations. However, with respect to the differential concentration-dependent response of the rBMECs to Cu-NP exposure (Figure 1), the induction of cell proliferation at lower concentrations could be due to an increase in ratio of GSH to total GHS at slightly increased Cu storage, potentially causing the induction of angiogenesis, and further investigations may be warranted to elucidate the mechanisms for the observed increased cellular proliferation.

Together, the data in the current report provides compelling evidence that systemic exposure to Cu-NPs can produce significant biological responses in cerebral microvascular endothelial cells. Cu-NPs may induce cerebral microvasculature dysfunction of the BBB *in vitro*. The interactions of Cu-NPs at the cerebral microvasculature may produce an initial cascade of proinflammatory mediators that can contribute to brain inflammation, potential neurotoxicity and subsequent changes in brain function.

## Future perspective

This report clearly demonstrates that Cu-NPs can cause dysfunction in the protective characteristics of the cerebral microvasculature at high concentrations. The increased permeability of the cerebral microvasculature is associated with the release of proinflammatory cytokines. However, at low concentrations, Cu-NPs increased cellular proliferation of the cerebral microvasculature that may promote neovascularization and wound healing, and further investigation may be warranted. Considering the various metal oxide NPs that are currently used in the manufacturing of hundreds of commercial, industrial and medical products from a toxicological stand point, a vital key is to ascertain any potential health benefits and risks associated with these advances in technology. The industrial, commercial and medical use of nanotechnology will develop many new exciting technologies and we need to clearly understand how biological systems respond to exposure of these.

### Financial & competing interests disclosure

*This research was supported, in part, by an appointment to the Postgraduate Research Participation Program with the US Air Force Research Laboratory at the National Center for Toxicological Research/US FDA (AR, USA) administered by the Oak Ridge Institute of Science and Education (TN, USA) through an interagency agreement between the US Department of Energy, US Air Force Research Laboratory/RHPB and the FDA. Furthermore, the authors are responsible for the content and writing of the manuscript and do not necessarily reflect the position of the US Government or FDA, nor does mention of trade*

### Executive summary

***The effects of copper nanoparticles were tested in an* in vitro *model of the blood–brain barrier***

- Primary brain microvessel endothelial cells (BMECs) were isolated from rat cerebral cortices and cultured into confluent monolayers.

***The effects of copper nanoparticles on cellular proliferation in primary rat BMECs***

- Low concentrations (~3.13 μg/ml and below) significantly increased the cellular proliferation for both 40- and 60-nm sized copper nanoparticles (Cu-NPs). Conversely, higher concentrations (~12.5 μg/ml and above) significantly reduced cellular proliferation for both sized Cu-NPs. The observed lethal dose for 50% was approximately 12.5 μg/ml for both sizes of Cu-NPs. Lower doses of Cu-NPs significantly increased cellular proliferation and may promote neovascularization and wound healing.

***The effects of Cu-NPs on the release of prostaglandin $E_2$***

- The release of prostaglandin $E_2$ from the rat BMEC (rBMEC) monolayers was evaluated at various time intervals (0–8 h) following exposure to Cu-NPs (40 and 60 nm), and significant increases in extracellular levels of prostaglandin $E_2$ (~threefold) were observed.

***The effects of Cu-NPs on the extracellular concentrations of cytokines***

- Significant amounts (~threefold) of TNF-α were released from the rBMECs following treatment with both 40- and 60-nm Cu-NPs. The release of IL-1β from rBMECs was robust in response (~fivefold) to both sized Cu-NPs.

***Morphology of rBMECs following exposure to Cu-NPs***

- The micrographs of rBMECs following treatment with Cu-NPs exhibited significant morphological changes when compared with control monolayers after 24 h of exposure.

***Cu-NP exposure affects permeability of rBMECs***

- Both sized Cu-NPs significantly increased the permeability of fluorescein (~twofold) across the rBMEC monolayers. Higher doses of Cu-NPs significantly altered cellular morphology of rBMECs and increased the permeability of rBMECs to fluorescein.

*names or commercial products constitute endorsement or recommendation for use. The authors have no other relevant affiliations or financial involvement with any organization or entity with a financial interest in or financial conflict with the subject matter or materials discussed in the manuscript apart from those disclosed.*

*No writing assistance was utilized in the production of this manuscript.*

## Ethical conduct of research

*The authors state that they have obtained appropriate institutional review board approval or have followed the principles outlined in the Declaration of Helsinki for all human or animal experimental investigations. In addition, for investigations involving human subjects, informed consent has been obtained from the participants involved.*

## References


Papers of special note have been highlighted as:
- ▪ of interest
- ▪▪ of considerable interest

1 Aruoja V, Dubourguier HC, Kasemets K, Kahru A. Toxicity of nanoparticles of CuO, ZnO and $TiO_2$ to microalgae *Pseudokirchneriella subcapitata*. *Sci. Total Environ.* 407(4), 1461–1468 (2009).

2 Hussain SM, Braydich-Stolle LK, Schrand AM *et al.* Toxicity evaluation for safe use of nanomaterials: recent achievements and technical challenges. *Adv. Mater.* 21(16), 1549–1559 (2009).

3 Schrand AM, Rahman MF, Hussain SM, Schlager JJ, Smith DA, Syed AF. Metal-based nanoparticles and their toxicity assessment. *Wiley Interdiscip. Rev. Nanomed. Nanobiotechnol.* 2(5), 544–568 (2010).

4 Sharma HS, Ali SF, Hussain SM, Schlager JJ, Sharma A. Influence of engineered nanoparticles from metals on the blood–brain barrier permeability, cerebral blood flow, brain edema and neurotoxicity. An experimental study in the rat and mice using biochemical and morphological approaches. *J. Nanosci. Nanotechnol.* 9(8), 5055–5072 (2009).

▪▪ **Evaluates blood–brain barrier permeability alterations of metallic colloidal nanoparticles *in vivo*.**

5 Sharma HS, Ali SF, Tian ZR *et al.* Chronic treatment with nanoparticles exacerbate hyperthermia induced blood–brain barrier breakdown, cognitive dysfunction and brain pathology in the rat. Neuroprotective effects of nanowired–antioxidant compound H-290/51. *J. Nanosci. Nanotechnol.* 9(8), 5073–5090 (2009).

▪▪ **Evaluates blood–brain barrier permeability alterations of metallic colloidal nanoparticles *in vivo*.**

6 Claudio L, Martiney JA, Brosnan CF. Ultrastructural studies of the blood–retina barrier after exposure to interleukin-1β or tumor necrosis factor-α. *Lab. Invest.* 70(6), 850–861 (1994).

7 de Vries HE, Blom-Roosemalen MC, van Oosten M *et al.* The influence of cytokines on the integrity of the blood–brain barrier *in vitro*. *J. Neuroimmunol.* 64(1), 37–43 (1996).

8 Deli MA, Descamps L, Dehouck MP *et al.* Exposure of tumor necrosis factor-α to luminal membrane of bovine brain capillary endothelial cells cocultured with astrocytes induces a delayed increase of permeability and cytoplasmic stress fiber formation of actin. *J. Neurosci. Res.* 41(6), 717–726 (1995).

9 Mark KS, Trickler WJ, Miller DW. Tumor necrosis factor-α induces cyclooxygenase-2 expression and prostaglandin release in brain microvessel endothelial cells. *J. Pharmacol. Exp. Ther.* 297(3), 1051–1058 (2001).

10 Bove K, Neumann P, Gertzberg N, Johnson A. Role of ecNOS-derived NO in mediating TNF-induced endothelial barrier dysfunction. *Am. J. Physiol. Lung Cell Mol. Physiol.* 280(5), L914–L922 (2001).

11 Vadeboncoeur N, Segura M, Al-Numani D, Vanier G, Gottschalk M. Pro-inflammatory cytokine and chemokine release by human brain microvascular endothelial cells stimulated by *Streptococcus suis serotype* 2. *FEMS Immunol. Med. Microbiol.* 35(1), 49–58 (2003).

12 Mayhan WG. Cellular mechanisms by which tumor necrosis factor-α produces disruption of the blood–brain barrier. *Brain Res.* 927(2), 144–152 (2002).

▪▪ **Reviews the link between proinflammatory cytokines and both increased cerebral microvascular permeability and dysfunction in the restrictive nature of the blood–brain barrier.**

13 Abraham CS, Deli MA, Joo F, Megyeri P, Torpier G. Intracarotid tumor necrosis factor-α administration increases the blood-brain barrier permeability in cerebral cortex of the newborn pig: quantitative aspects of double-labelling studies and confocal laser scanning analysis. *Neurosci. Lett.* 208(2), 85–88 (1996).

14 Buttini M, Limonta S, Boddeke HW. Peripheral administration of lipopolysaccharide induces activation of microglial cells in rat brain. *Neurochem. Int.* 29(1), 25–35 (1996).

15 Saito K, Suyama K, Nishida K, Sei Y, Basile AS. Early increases in TNF-α, IL-6 and IL-1β levels following transient cerebral ischemia in gerbil brain. *Neurosci. Lett.* 206(2–3), 149–152 (1996).

16 Shalev H, Serlin Y, Friedman A. Breaching the blood–brain barrier as a gate to psychiatric disorder. *Cardiovasc. Psychiat. Neurol.* 278531 (2009).

17 Audus KL, Borchardt RT. Bovine brain microvessel endothelial cell monolayers as a model system for the blood–brain barrier. *Ann. NY Acad. Sci.* 507, 9–18 (1987).

▪ **Methodology of isolating the bovine cerebral microvessel endothelial cells used to isolate the rat brain microvessel endothelial cell model of the blood–brain barrier.**

18 Franke H, Galla H, Beuckmann CT. Primary cultures of brain microvessel endothelial cells: a valid and flexible model to study drug transport through the blood–brain barrier *in vitro*. *Brain Res. Protoc.* 5(3), 248–256 (2000).

19 Franke H, Galla HJ, Beuckmann CT. An improved low-permeability *in vitro*-model of the blood–brain barrier: transport studies on retinoids, sucrose, haloperidol, caffeine and mannitol. *Brain Res.* 818(1), 65–71 (1999).

20 Weber SJ, Abbruscato TJ, Brownson EA *et al.* Assessment of an *in vitro* blood–brain barrier model using several [Met5] enkephalin opioid analogs. *J. Pharmacol. Exp. Ther.* 266(3), 1649–1655 (1993).

21 Trickler WJ, Lantz SM, Murdock RC *et al.* Silver nanoparticle induced blood–brain barrier inflammation and increased permeability in primary rat brain microvessel endothelial cells. *ToxSci. Adv. Access* 118(1), 160–170 (2010).

▪▪ **Evaluates the toxicity and permeability of silver nanoparticles in the rat brain microvessel endothelial cell model of the blood–brain barrier.**

22 Trickler WJ, Lantz SM, Murdock RC *et al.* Brain microvessel endothelial cells responses to gold nanoparticles: *in vitro* proinflammatory mediators and permeability. *Nanotoxicology* 5(4), 497–492 (2010).

▪▪ **Evaluates the toxicity and permeability of gold nanoparticles in the rat brain microvessel endothelial cell model of the blood–brain barrier.**

23 Trickler WJ, Mayhan WG, Miller DW. Brain microvessel endothelial cell responses to tumor necrosis factor-α involve a nuclear factor κB (NF-κB) signal transduction pathway. *Brain Res.* 1048(1–2), 24–31 (2005).

24 Karlsson J, Artursson P. A new diffusion chamber system for the determination of drug permeability coefficients across the human intestinal epithelium that are independent of the unstirred water layer. *Biochim. Biophys. Acta* 1111(2), 204–210 (1992).

25 Chen Z, Meng H, Xing G *et al.* Acute toxicological effects of copper nanoparticles *in vivo*. *Toxicol. Lett.* 163(2), 109–120 (2006).

26 Liu Y, Gao Y, Zhang L *et al.* Potential health impact on mice after nasal instillation of nano-sized copper particles and their translocation in mice. *J. Nanosci. Nanotechnol.* 9(11), 6335–6343 (2009).

27 Prabhu BM, Ali SF, Murdock RC, Hussain SM, Srivatsan M. Copper nanoparticles exert size and concentration dependent toxicity on somatosensory neurons of rat. *Nanotoxicology* 4(2), 150–160 (2010).

28 Freedman JH, Ciriolo MR, Peisach J. The role of glutathione in copper metabolism and toxicity. *J. Biol. Chem.* 264(10), 5598–5605 (1989).

29 Freedman JH, Peisach J. Intracellular copper transport in cultured hepatoma cells. *Biochem. Biophys. Res. Comm.* 164(1), 134–140 (1989).

30 Steinebach OM, Wolterbeek HT. Role of cytosolic copper, metallothionein and glutathione in copper toxicity in rat hepatoma tissue culture cells. *Toxicology* 92(1–3), 75–90 (1994).

31 Steinebach OM, Wolterbeek HT. Effects of copper on rat hepatoma HTC cells and primary cultured rat hepatocytes. *J. Inorg. Biochem.* 53(1), 27–48 (1994).

32 Fahmy B, Cormier SA. Copper oxide nanoparticles induce oxidative stress and cytotoxicity in airway epithelial cells. *Toxicol. In Vitro* 23(7), 1365–1371 (2009).

▪▪ **Demonstrated the cytotoxic effects of metal oxides that are not due to the solubility of the transition metal.**

33 Karlsson HL, Cronholm P, Gustafsson J, Moller L. Copper oxide nanoparticles are highly toxic: a comparison between metal oxide nanoparticles and carbon nanotubes. *Chem. Res. Toxicol.* 21(9), 1726–1732 (2008).

34 Karlsson HL, Gustafsson J, Cronholm P, Moller L. Size-dependent toxicity of metal oxide particles – a comparison between nano- and micrometer size. *Toxicol. Lett.* 188(2), 112–118 (2009).

35 Li N, Sioutas C, Cho A *et al.* Ultrafine particulate pollutants induce oxidative stress and mitochondrial damage. *Environ. Health Perspect.* 111(4), 455–460 (2003).

36 Xia T, Kovochich M, Nel AE. Impairment of mitochondrial function by particulate matter (PM) and their toxic components: implications for PM-induced cardiovascular and lung disease. *Front. Biosci.* 12, 1238–1246 (2007).

37 Hartung HP, Jung S, Stoll G *et al.* Inflammatory mediators in demyelinating disorders of the CNS and PNS. *J. Neuroimmunol.* 40(2–3), 197–210 (1992).

38 Duchini A. The role of central nervous system endothelial cell activation in the pathogenesis of hepatic encephalopathy. *Med. Hypotheses.* 46(3), 239–244 (1996).

39 Fiala M, Looney DJ, Stins M *et al.* TNF-α opens a paracellular route for HIV-1 invasion across the blood–brain barrier. *Mol. Med.* 3(8), 553–564 (1997).

40 Calingasan NY, Huang PL, Chun HS, Fabian A, Gibson GE. Vascular factors are critical in selective neuronal loss in an animal model of impaired oxidative metabolism. *J. Neuropathol. Exp. Neurol.* 59(3), 207–217 (2000).

41 Ergenekon E, Gucuyener K, Erbas D, Aral S, Koc E, Atalay Y. Cerebrospinal fluid and serum vascular endothelial growth factor and nitric oxide levels in newborns with hypoxic ischemic encephalopathy. *Brain Dev.* 26(5), 283–286 (2004).